Science of the Total Environment 803 (2022) 149889

Contents lists available at ScienceDirect

Science of the Total Environment

journal homepage: www.elsevier.com/locate/scitotenv

Snow cover persistence reverses the altitudinal patterns of warming above and below 5000 m on the Tibetan Plateau

Hongbo Zhang [a,b,c,d], W.W. Immerzeel [c], Fan Zhang [b,e,f,*], Remco J. de Kok [c], Deliang Chen [g], Wei Yan [h]

[a] College of Water Resources & Civil Engineering, China Agricultural University, Beijing, China
[b] State Key Laboratory of Tibetan Plateau Earth System, Resources and Environment (TPESRE), Institute of Tibetan Plateau Research, Chinese Academy of Sciences, Beijing 100101, China
[c] Utrecht University, Department of Physical Geography, PO Box 80115, Utrecht, the Netherlands
[d] State Key Laboratory of Hydrology-Water Resources and Hydraulic Engineering, Nanjing Hydraulic Research Institute, Nanjing, China
[e] CAS Center for Excellence in Tibetan Plateau Earth Sciences, Beijing, China
[f] University of Chinese Academy of Sciences, Beijing, China
[g] Regional Climate Group, Department of Earth Sciences, University of Gothenburg, Gothenburg, Sweden
[h] School of Geographic Sciences, Xinyang Normal University, Xinyang, China

HIGHLIGHTS

- A novel 1-km air temperature dataset with high accuracy is used for warming analysis.
- The well-established snow-albedo feedback is less important at high elevations.
- The persistent snow cover prohibits an increase of warming above 5000 m.

GRAPHICAL ABSTRACT

Fig. Elevation dependent warming affected by snow cover and glaciers. Warming rate of air temperature and as function of elevation and snow cover days with glacierized pixels excluded (a). Comparison of warming rates between non-glacierized and glacierized areas (b).

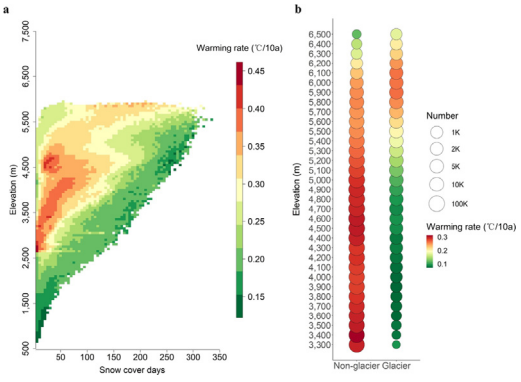

ARTICLE INFO

Article history:
Received 19 May 2021
Received in revised form 16 August 2021
Accepted 20 August 2021
Available online 30 August 2021

Editor: Jay Gan

Keywords:
Tibetan Plateau
Elevation dependent warming
Climate change
Feedback of snow and glaciers

ABSTRACT

The Tibetan Plateau (TP) is a global warming hotspot, however, the warming status at high elevation (>5000 m) is poorly understood due to very sparse observations. Here we analyze spatial patterns in TP warming rates based on a novel near-surface air temperature dataset of 1980–2014 recently developed by ingesting high-elevation observations and downscaled reanalysis datasets. We show that the high snow cover persistence at high elevation reduces strengthening of positive feedbacks responsible for elevation dependent warming at low-middle elevations, leading to reversed altitudinal patterns of TP warming above and below 5000 m. An important negative feedback is induced by the presence of snow and glaciers at elevations above 5000 m, due to their "buffering" effects by consuming or reflecting energy that would be used for warming in the absence of snow or ice. A further decrease in snow cover and glacier extent at high elevations may thus amplify the warming on the TP.

* Corresponding author at: State Key Laboratory of Tibetan Plateau Earth System, Resources and Environment (TPESRE), Institute of Tibetan Plateau Research, Chinese Academy of Sciences, Beijing 100101, China.
E-mail address: Zhangfan@itpcas.ac.cn (F. Zhang).

https://doi.org/10.1016/j.scitotenv.2021.149889
0048-9697/

1. Introduction

The Tibetan Plateau (TP) with an average elevation of >4000 m has great thermal and dynamical influence on regional and even global circulation systems such as the Asian monsoon (Wu et al., 2007). The TP has warmed much faster than the global average in recent decades (Guo and Wang, 2012; You et al., 2021) and it has been considered as a typical case of the phenomenon called elevation dependent warming (EDW) (Pepin et al., 2015). Observed environmental changes on the TP due to this rapid warming are well documented, in particular extensive glacier receding (Yao et al., 2012), permafrost degradation (Cheng and Wu, 2007) and lake expansion (Zhang et al., 2019). Considering that the TP is the "water tower" of Asia providing water for millions of people downstream (Immerzeel et al., 2010), a detailed understanding of warming and possible feedback mechanisms is of great importance for regional water security.

EDW studies on the TP show that the warming rate generally increases with altitude <5000 m, and that it may not increase further at higher altitudes (Gao et al., 2018; Guo et al., 2019a; Li et al., 2020; Liu and Chen, 2000; Qin et al., 2009). Due to the high elevations and extreme conditions on the North-western part of the TP, the observational network is biased towards the South-east and elevations <5000 m. The warming status in the North-western part and at high elevation (>5000 m) therefore remains unquantified. Climate models, reanalysis (Gao et al., 2018; Palazzi et al., 2019) and remotely sensed land surface temperatures (Guo et al., 2019a; Pepin et al., 2019; Qin et al., 2009) have also been used to quantify spatial variation in warming rates. However, their low resolution, high uncertainty and/or short duration hamper the understanding of long-term spatiotemporal temperature trends on the TP and the detection of underlying mechanisms. Some high-resolution air temperature datasets have also been developed recently by downscaling reanalysis (Ding et al., 2018) or Climatic Research Unit (CRU) (Peng et al., 2019) data while they lack training and validation data from independent high-elevation stations, especially for glacierized regions.

Snow (Guo et al., 2019b; Palazzi et al., 2019), clouds (Hua et al., 2018; Yang et al., 2018), water vapor, aerosols (Kang et al., 2019), land use and vegetation (Liu et al., 2019; Shen et al., 2015) may be possible factors controlling EDW on the TP with their importance varying seasonally or interannually (Gao et al., 2019; You et al., 2020). Among them, snow cover change is considered as one of the most important factor affecting the altitudinal pattern of TP warming, known as the snow albedo feedback mechanism (Guo et al., 2019a; Guo et al., 2019b; Guo et al., 2016; Palazzi et al., 2017; Palazzi et al., 2019; Pepin et al., 2015; Rangwala et al., 2010). Due to the high albedo of snow, snow covered surface can reflect much solar radiation. The strongest warming is expected around the 0 °C isotherm where the snowline is retreating (Pepin et al., 2015). Remote sensing temperature data show that the fastest warming occurs around 5000 m, which is well within the elevation ranges of snow line of the TP (Pepin et al., 2019; Qin et al., 2009). Based on station observations, Guo et al. (2021) also found an accelerating decrease of snow depth at elevations of 4000–5000 m. However, the short availability of high-resolution remote sensing data and limited altitudinal representativeness of station observations inhibit the understanding of the effects of snow cover on EDW at higher elevations.

For overcoming these problems, we have recently developed a machine learning-based approach to create a novel 1-km daily near-surface air temperature time series from 1980 to 2014 by combining eight reanalysis datasets and data from 113 weather stations including 13 unique sites at high elevation (see Fig. 1a and Section 2.1) (Zhang et al., 2021). Here, we use this dataset to detect temporal trends in the warming rate and to identify and explain EDW patterns.

2. Materials and methods

2.1. Air temperature dataset and other data sources for distributions of elevation, glacier, snow cover days and cloud coverage

A new 1-km daily mean air temperature dataset during 1980–2014 was used for analyzing TP warming. It was created generally following three steps: spatially continuous multiyear average monthly air temperature lapse rates were first estimated mainly based on MODIS LST data; then, the MODIS-estimated temperature lapse rates were used for downscaling eight major reanalysis air temperature datasets with varying resolutions (0.25° to 2.0°) to 1-km resolution; finally, the eight downscaled reanalysis data together with five auxiliary variables were taken as predictors in a machine learning model (i.e., Gradient Boosting) that was trained and validated using numerous observations from 100 "common stations" and 13 "high-elevation stations" (Fig. 1). "Common station" represents CMA station. "High-elevation station" represents the stations set up in the field at generally higher elevations than their neighboring common stations. The elevations of high-elevation stations were all higher than the average altitude (~3300 m) of the 100 common stations (Zhang et al., 2021). The detailed information about how the dataset was developed and evaluated can be found in Zhang et al. (2021). The new dataset was demonstrated to have significantly better accuracy than all the original and downscaled reanalysis data, especially in high-elevation and glacierized areas based on the station-based cross-validation (Zhang et al., 2021).

Elevation information was derived from Shuttle Radar Topography Mission (SRTM) Digital Elevation Model (DEM) dataset, which was further spatially aggregated from its original resolution (~90 m) to ~1 km. The Randolph Glacier Inventory (RGI 6.0) dataset (Pfeffer et al., 2014) was used to separate glacierized areas from non-glacierized areas. The original resolution of the glacier data is ~30 m and was resampled to a coarser resolution of ~1 km which is the same as that of the new air temperature dataset. The multiyear average annual snow cover days were calculated from a cloud-free daily snow cover dataset of 2005–2013 developed by combining MODIS daily snow cover data and Interactive Multisensor Snow and Ice Mapping System (IMS) data (referred to as "MODIMS") (Yu et al., 2016). After removing cloud contamination, the overall accuracy of MODIMS was reported to be 94% based on daily snow depth observations from 105 stations across the TP. Though MODIMS has a short time span, its spatial resolution (~500 m) is sufficiently high. There are some other snow datasets with long availability such as the "long-term sequence dataset of China snow depth" (Che et al., 2008; Dai et al., 2012) (referred to as "LCSD") and the Global Snow Monitoring for Climate Research (GlobSnow) snow water equivalent dataset (Liyun and Tao, 2015; Takala et al., 2011), however, their spatial resolutions are generally much lower (≥25 km) and are not able to accurately capture the altitudinal distributions of snow cover. Two kinds of data sources were used for calculating long-term (1980–2014) snow cover trends, the most important of which were the daily snow depth observations from 32 CMA stations with continuous records during 1980–2013 were used for detecting long-term trends of snow cover days (SCD). It should be noted that for snow depth, though there were 100 CMA stations on the TP, there were many missing snow depth observations in some stations. Thus, the stations with the percentage of missing snow depth observations >1% were excluded and totally 32 stations were left. As auxiliary, the daily snow depth data from LCSD of 1979–2018 at 0.25° resolution which were derived from the Scanning Multichannel Microwave Radiometer (SMMR, 1978–1987), Special Sensor Microwave/Imager (SSM/I, 1987–2008) and the Advanced Microwave Scanning Radiometer - Earth Observing System (AMSR-E, 2002–2010), and calibrated using long-term snow depth observations, were also used for calculating pixel-level trends of snow cover days, and only pixels with snow depth >1 cm were considered as snow covered. The multiyear average annual cloud coverage was derived from the "EarthEnv Global 1-km

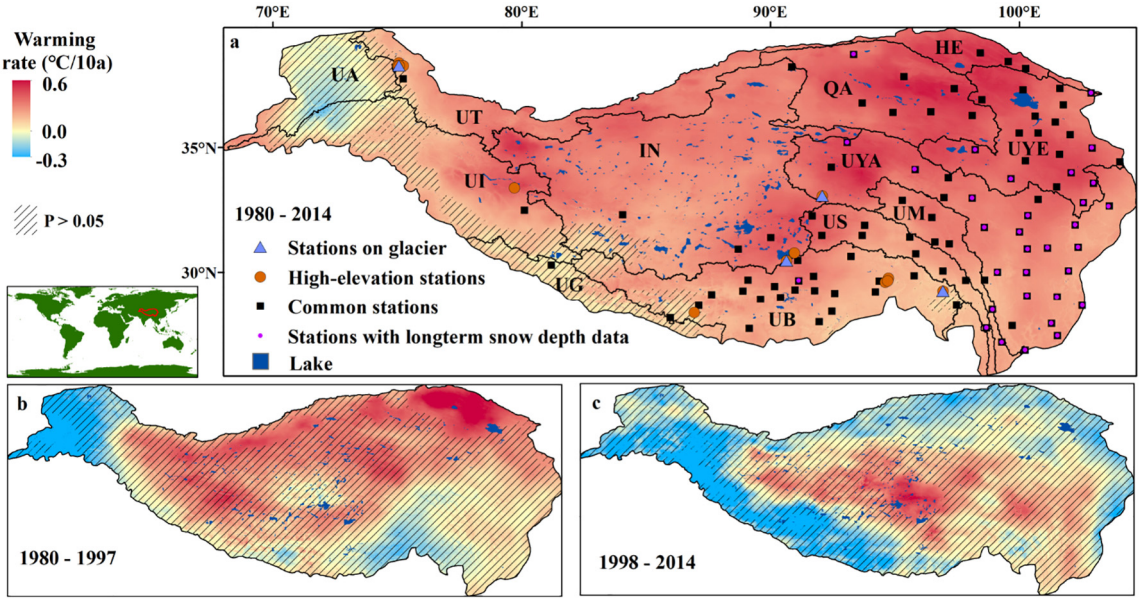

Fig. 1. The all-year warming rates of the Tibetan Plateau. 1980–2014 (a). 1980–1997 (b). 1998–2014 (c). UA: Upper Amu Dayra, UB: Upper Brahmaputra, UG: Upper Ganges, HE: Hexi, UI: Upper Indus, IN: Inner, UM: Upper Mekong, QA: Qaidam, US: Upper Salween, UT: Upper Tarim, UYA: Upper Yangtse, UYE: Upper Yellow, TP: the whole Tibetan Plateau. Shadowed area means insignificant temperature trends ($P > 0.5$).

Cloud Frequency Version 1" which integrated 15 years (i.e., 2000–2014) of cloud observations from MODIS (Wilson and Jetz, 2016). The multi-year average annual normalized difference vegetation index (NDVI) was calculated from the TERRA MODIS Vegetation Indices (MOD13A3) Version 6 product (Didan et al., 2015).

2.2. Statistical analysis of TP warming

The warming rate of each air temperature pixel was calculated based on a linear regression between the yearly temperatures of the pixel and the time series (i.e., years 1980–2014) and the significance level (*P*-value) was calculated based on the *t*-test. Since TP warming is closely related to regional water availability, a basin-scale analysis was also conducted by spatially aggregating the pixel-level warming rates to 12 sub-regions, which were defined as 12 major river basins across the TP (Fig. 1a). For analyzing the mechanism driving the temperature change of the TP, the trends of yearly SCD were calculated following the same way. The sequential Mann-Kendall test was used for detecting the turning point in the time series of yearly SCD based on daily snow depth observations from stations. It generally calculates a positive (UF) and an inverse (UB) series of Kendall normalized tau's, and the crossing points of them within the confidence limits are considered as turning points.

A number of studies have focused on the relationship between snow cover trends and warming rates on the TP (Guo et al., 2019a; Guo et al., 2019b; Guo et al., 2016; Palazzi et al., 2017; Pepin et al., 2015; Rangwala et al., 2010), however, the climatology state of snow cover may also have important effects. For example, a global climate model simulation study has recently predicted enhanced warming in spring and autumn for the TP due to more snow-covered areas transitioned to be snow-free (Palazzi et al., 2019). To investigate the effects of elevation and snow cover persistence on warming rates, temperature trends were grouped by elevation and SCD. 160 kinds of elevation conditions were defined by making elevation varying from 500 m to 8500 m with an interval of 50 m. 73 kinds of SCD climatology (i.e., the multiyear average yearly SCD) conditions were defined by making SCD ranging from 0 to 365 days with an interval of 5 days. All pixels were then assigned to different elevation-SCD groups (number = 160 × 73) and for each group, the warming rates were averaged. To reduce the uncertainty, pixels with insignificant (*P*-value > 0.05) temperature trends were removed and the groups with number of valid pixels <50 were not considered. Finally, a total of 3889 elevation-SCD groups were left. Because 99.9% of all pixels had elevations <6500 m based on the 1-km DEM data used here, there was no group with elevation >6500 m meeting the requirements. The 2-way analysis of variance (ANOVA) was further used to quantify the contributions of elevation and snow cover persistence to the variances of TP warming (Zhang et al., 2019). However, its results can be greatly affected by the order of independent variables if the number of variables is greater than one and the samples are unbalanced (like in our study) (Hector et al., 2010). To overcome this problem, four square sub-regions (i.e., Regions I, II, III and IV) with orthogonal samples of elevation and SCD are created to fit in as many square boxes as possible to the envelope on each of the panels for each of the major basins (including the whole TP). fit in as many square boxes as possible to the envelope on each of the panels The two-way ANOVA was then conducted in each sub-region, and the weighted average contributions based on all the four sub-regions according to their sample number are reported for the corresponding basin. Since only orthogonal samples were used for doing ANOVA and some samples are thus dropped, the linear regression models that consider all the samples were also implemented for checking the effects of elevation and SCD on explaining the variation of warming rates. The R-Squared was calculated to measure the proportion of the variance for warming rates explained by the regression model.

Because cloud cover (Hua et al., 2018) and vegetation (Shen et al., 2015) may also influence the TP warming as previously reported, the partial least squares path modeling (PLS-PM) was further used for testing the relative effects of elevation and climatology conditions of snow cover, vegetation and cloud cover in modulating the spatial distribution of warming rates. PLS-PM is widely used in social and ecological sciences for integrating complex interrelationships among different factors (Nie et al., 2019). The PLS-PM (Sanchez, 2013) produces a path diagram constructed by different variables linking with each other. A path coefficient represents the direct effect of a variable on another one. An indirect effect of one variable on another one (i.e., there is a third variable between them in the path) can be obtained by multiplying the

coefficients of the indirect paths. The total effect is the sum of indirect and direct effects. Path coefficients were solved iteratively based on ordinary least squares.

3. Results and discussions

3.1. Spatial and temporal pattern of warming

The TP has warmed very rapidly during the period 1980–2014 with a spatially average rate of about 0.29 ± 0.13 °C/decade (Fig. 1a) and this rate is much higher than the global average (0.17 °C/decade) (Team, 2016) for the same period. However, there were large spatial differences in warming rate on the TP itself too. The northern part showed higher warming rates than the southern part as previously reported (Duan et al., 2015) and the eastern part warmed much faster than the western part. There are even considerable areas with insignificant or even negative trends in the western TP which is partly consistent with summer cooling found in upper Indus (Fowler and Archer, 2006) though contradicting some earlier work (Liu and Chen, 2000). Although the observational basis to train the machine learning algorithm in this region is limited, our results are remarkably consistent with a region where glaciers showed neutral or even slightly positive mass balance, commonly referred to as the "Karakoram anomaly" (Brun et al., 2017; Gardelle et al., 2012; Hewitt, 2005; Kapnick et al., 2014; Yao et al., 2012).

Ten of the total 12 major basins of the TP showed significant warming in annual temperature during the period except for Upper Amu and Upper Ganges (UG) (see Fig. 2). The lack of significant warming in UG was probably caused by the occurrence of erratically cold years between 2011 and 2014 and is partly consistent with a recent study reporting southwestern cooling (since 2001) in the TP (Guo et al., 2019b). If the period 1980–2010 was considered then UG also showed significant warming, although the results are not shown here. There were also distinct seasonal differences (Fig. 2). For the whole TP, the strongest warming (~0.31 ± 0.14 °C/decade) occurred in winter and the other three seasons showed nearly equal warming rates. However, the seasonal warming patterns differed strongly between basins and some clear regional patterns can be distinguished. For the three most southeastern basins (i.e., Upper Mekong, Upper Salween, and Upper Yangtse), the warming in winter was the strongest and weakest in autumn, whereas the reversed pattern was observed for the most western basins (i.e., Upper Amu, Upper Tarim and Upper Indus).

Based on relatively dense stations, the EDW pattern below 5000 m has been well established that the TP warming at higher elevations (>2000 m) is significantly higher than that at lower elevations (≤2000 m) (Guo et al., 2021). This pattern is also consistent with our finding (Fig. 3a). The very high warming rates at 2500–3000 m are also consistent with several studies that identified the fastest warming in the Northern part of the plateau, especially in the Qaidam (QA) (Fig. 1a), but at a relatively low elevation of around 3000 m. They attributed this violation of the EDW hypothesis to decreasing stratospheric ozone and precipitation (Duan et al., 2015; Guo and Wang, 2012). What we bring here is some new evidence about the 35-year warming trends for elevations >5000 m, thanks to the high spatial resolution of our new air temperature data (Fig. 3a). The warming rate gradually decreased at elevations between 5000 and 8000 m, which is roughly consistent with a decreasing trend in the warming rates (1983–2011) at elevations ranging from 5000 to 6000 m simulated by the Weather Research and Forecasting model (Gao et al., 2018) and a rapid decrease of the warming rates (2001–2015) at elevations >4500 m based on the air temperature data estimated from MODIS (Guo et al., 2019a).

3.2. Buffering effects of snow cover persistence on warming

Due to the high spatial resolution of the new air temperature data, detailed warming rates as function of elevation and SCD can be quantified (Fig. 4a). For low snow cover areas (SCD < ~125), along the vertical direction of Fig. 4a, the warming rate indeed increased until a peak elevation and then decreased. The peak elevation gradually increased from ~2700 m when snow cover was low (SCD < 5), to over 6000 m when snow cover was persistent (SCD ≥ ~215). The SCD trends from the satellite-based snow depth dataset are found highly consistent with the warming trends varying with elevations, especially for areas with short SCD persistence where two peak regions of decreasing trends in SCD can be identified, though the SCD trends seem to be fragmented and the peak elevation of SCD trends seems somewhat higher than that of warming trends which could be affected by the coarser

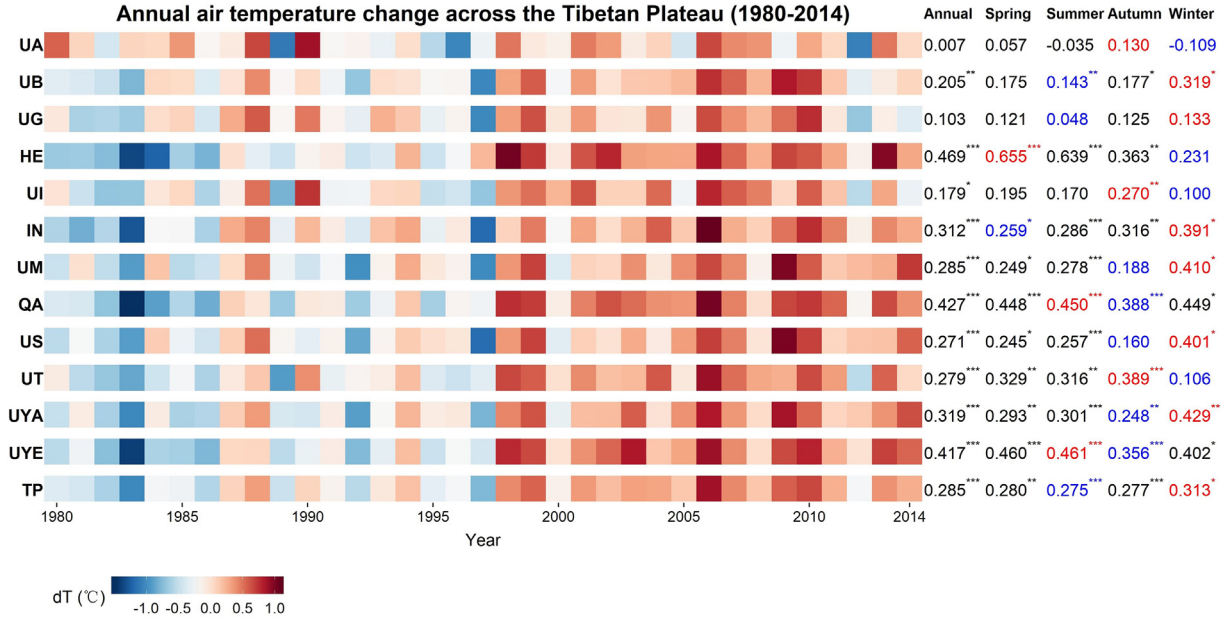

Fig. 2. Annual air temperature variations (colors) and trends (numbers on the right) across the TP (1980–2014). dT is the temperature anomaly relative to the average temperature during 1980–2014 for the corresponding basin. The significance levels of the trends are indicated by ***: $P < 0.001$; **: $P < 0.01$; *: $P < 0.05$. Number in red indicates the season with the highest warming rate; number in blue means the season with the smallest warming rate.

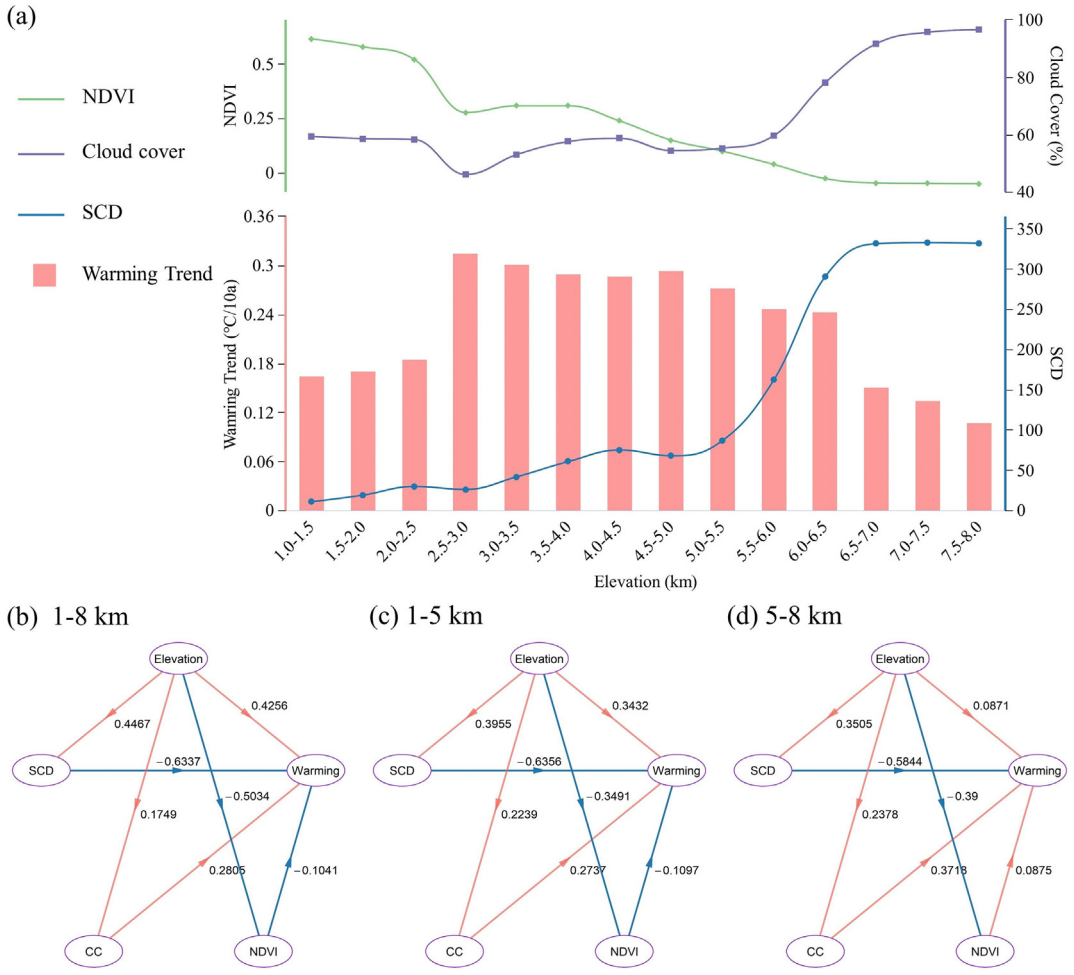

Fig. 3. The altitudinal distribution of warming rate, multiyear average snow cover days (SCD), NDVI and cloud cover (a), and the partial least squares path model (PLS-PM) of vegetation (NDVI), snow cover (SCD), elevation and cloud cover (CC) effects on the TP warming for elevations of 1000–8000 m (b), 1000–5000 m (c) and 5000–8000 m (d). In panels (b) – (d), the red and blue arrows represent the positive and negative effects, respectively. Note that all the path coefficients are statistically significant ($P < 0.05$) in panels (b)–(d).

resolution (0.25°) (Fig. 5 and Section 2.1). This indicates that there may be a strong feedback between snow cover depletion and EDW, which is consistent with previous studies considering snow-albedo feedback as a key control for EDW (Guo et al., 2019a; Guo et al., 2016; Pepin et al., 2015). It should be noted that the x-axis of Fig. 4a represents the average state of SCD (see Section 2.2) and does not mean that SCD is constant during the study period.

A recent modeling study shows that this snow-albedo feedback is active for the low-middle range of elevations over the TP where snow cover experiences strong seasonal changes (Niu et al., 2021). However, over high elevations, snow and ice hardly change, making the snow-albedo feedback insignificant. Another new finding is that at a given elevation, the warming rate decreased with an increasing snow persistence (Fig. 4). Snow cover showed a "buffering" effect on warming as the presence of snow consumes energy for melting and reflects a large proportion of shortwave radiation. These processes conspire and lead to less net available energy for the sensible heat flux. This indicates that warming rates cannot be explained solely by elevation, as snow covers in low-middle elevations are variable, while for high elevations snow cover is much more persistent. It is also inspiring that a similar pattern emerges for most of major basins as shown in Fig. 6 only except QA and IN. The obviously different patterns of QA and IN compared with other basins could be related with their aridity. For example, the much lower peak elevation of warming at 2500–3000 m in QA could be related with the very low vegetation and cloud cover there (Fig. 3a).

The 2-way ANOVA based on orthogonal samples (see Section 2.2) showed that elevation was indeed more important than snow cover to explain the temperature change for all the 10 major basins. However, the effects of snow cover were also notable with its contributions >10% in Upper Brahmaputra, Upper Indus, Upper Salween and Upper Yangtse, and even >20% in Hexi, Upper Tarim and Upper Yellow (Fig. 7). The averaged contributions of elevation and snow cover to the variance of warming rates for the whole TP are 37.1% and 22.3%, respectively. It should be noted that the relatively large contribution of residuals (~29% for the whole TP) may indicate moderate effects from other factors such as cloud cover (Guo et al., 2019a). The great importance of snow cover for warming at different elevations was further verified by the results of a linear regression analysis using all samples showing that when only elevation was considered, only 14.7% of the total variance in warming rates on the TP could be explained, but when SCD was included, 61.1% could be explained. A similar analysis for each of the 10 major basins further supported our hypothesis and, in all cases, except Inner, including the SCD increased the percentage of explained variance considerably, although the results are not shown here. Thus, we conclude that EDW mainly deduced by snow cover depletion is only valid up to 5000 m, above which the buffering effects of snow could be dominant due to more widespread and persistent snow cover and prohibit strengthening of warming with increasing elevation, explaining the reversed altitudinal patterns of warming rates of above and below 5000 m on the TP. Following this, the significantly

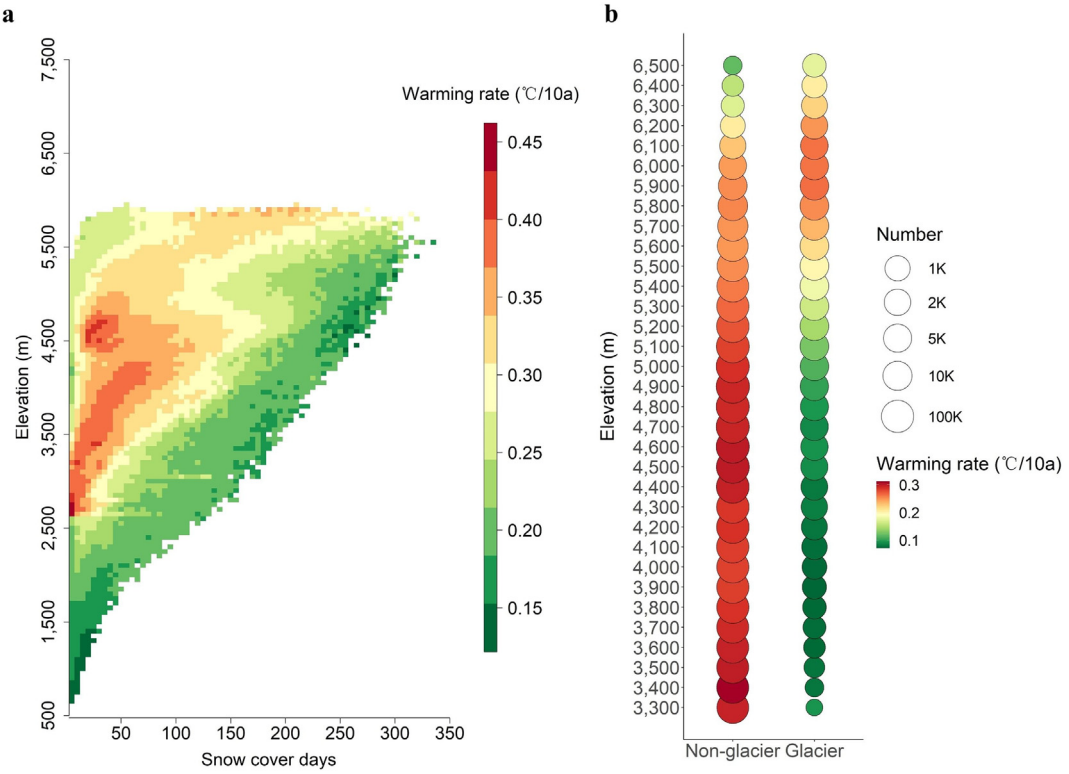

Fig. 4. Elevation dependent warming affected by snow cover and glaciers. Warming rate of air temperature and as function of elevation and snow cover days with glacierized pixels excluded (a). Comparison of warming rates between non-glacierized and glacierized areas (b).

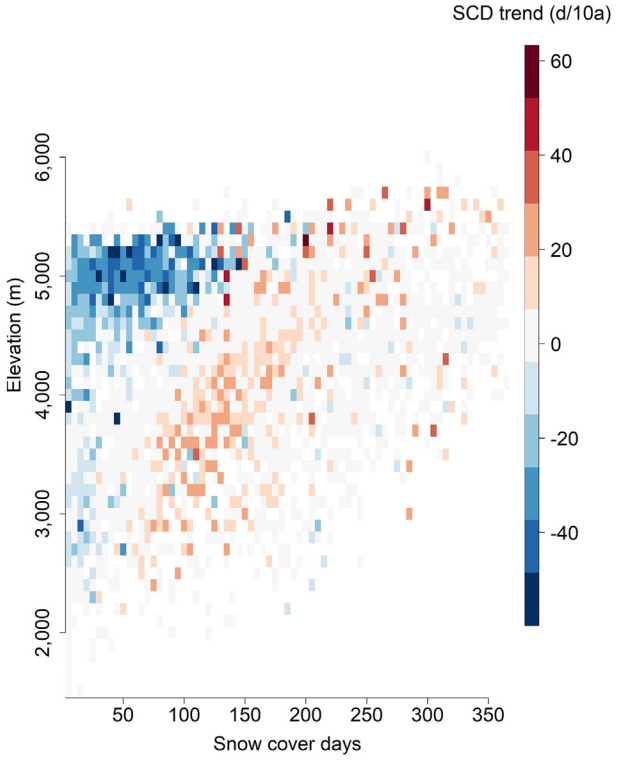

Fig. 5. Trends of snow cover days as function of elevation and multiyear average snow cover days. The snow cover days are calculated based on LCSD (see Section 2.1) data at the resolution of 0.25°.

lower SCDs of QA (34 versus 70 days) could be an important reason for explaining the earlier noted higher warming rate of QA basin compared with the TP average (0.43 versus 0.29 °C/decade).

Glaciers also play an important role in the TP water cycle. They are often covered by snow and the similarly high albedo and melt energy mechanism may suppress the warming rate. This is further verified by comparing the warming rates between glacierized and non-glacierized pixels (Fig. 4b). For almost all the elevation bands, the warming rates of glacierized areas were indeed much lower than those of non-glacierized areas. The region-wise warming rates of non-glacierized and glacierized areas were 0.29 and 0.17 °C/decade, respectively. It may be surprising that EDW seemed to disappear for non-glacierized regions (Fig. 4b). This is due to the lumped "disturbing" effects of snow cover. In fact, EDW was clearly shown when snow cover persistence was considered with glacier pixels removed (Fig. 4a). This could also explain why non-significant correlation between warming and elevation was found in some other studies (You et al., 2008). The altitudinal pattern of warming on glaciers seemed very different from that of non-glacierized areas. EDW was evident on glaciers with the warming rate consistently increasing from lower elevations to around 6000 m. This could be explained by the mass balance gradients of glaciers, i.e., more ablation occurred at lower altitudes as evidenced in several glaciers over the TP (Lin et al., 2017; Yang et al., 2013) and thus more energy was consumed. This could also be one reason why the peak elevation of warming for areas with high snow cover was up to 5000–6000 m (Fig. 4a) considering that no obvious dependence of SCD variation on elevation was found there (Fig. 5). However, for very high (>6000 m) glacier areas, the warming rate decreased with elevation, possibly due to the dominant effects of clouds, as indicated by a steep increase of cloud coverage above 6000 m (Fig. 3a). This finding indicates that also for glaciers, warming rates were buffered by ice because of ice and a large proportion of the energy was used for melt instead of warming the air. Hence, there is a feedback between glacier

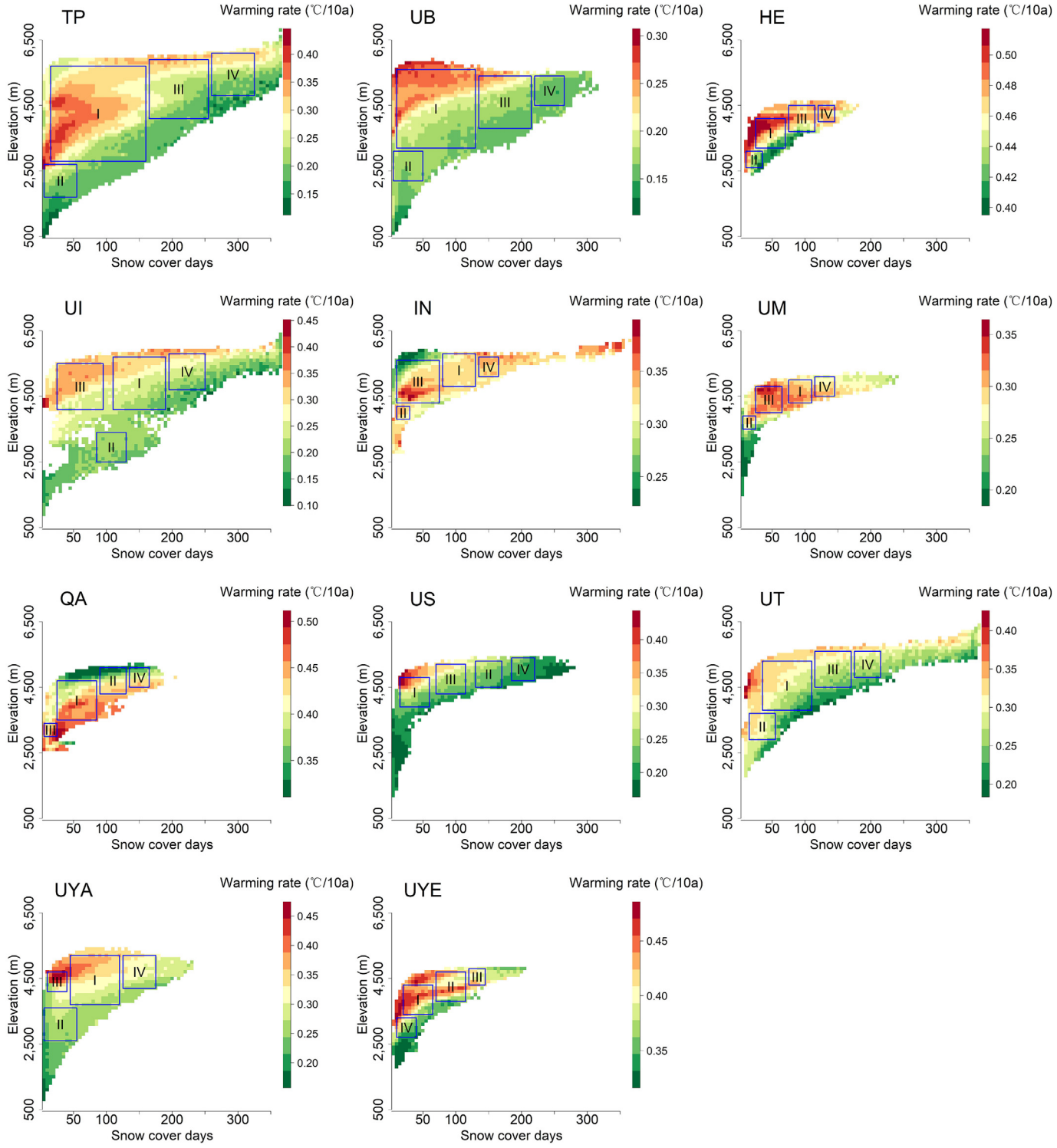

Fig. 6. Definition of sub regions (i.e., Regions I, II, III and IV) used in analysis of variance (ANOVA) of warming rates for the whole TP and 10 major basins. The blue squares delineate the pixels used for doing ANOVA with the region number displayed on top. Note: Those for UA and UG with most pixels showing insignificant trends are not shown here due to insufficient samples.

retreat and enhanced warming and this should be accounted for in future studies.

3.3. The possible mechanisms of different warming patterns below and above 5000 m

In addition to elevation and snow cover persistence, vegetation conditions and cloud cover persistence may also have effects on the spatial pattern of TP warming. For example, the abrupt increase in warming rates for elevations from 2000 to 3000 m is well along with the sharp decreases in NDVI and cloud cover (Fig. 3a), implying possibly important effects of vegetation (less vegetation leads to decreased surface albedo and less evaporate cooling) (Shen et al., 2015) and clouds (less clouds in the daytime bring more insolation) (Duan and Wu, 2006) on the warming (Fig. 3a). Similarly, the rapid decrease in warming rates at elevations from 6000 to 7000 m could be related with altitudinal

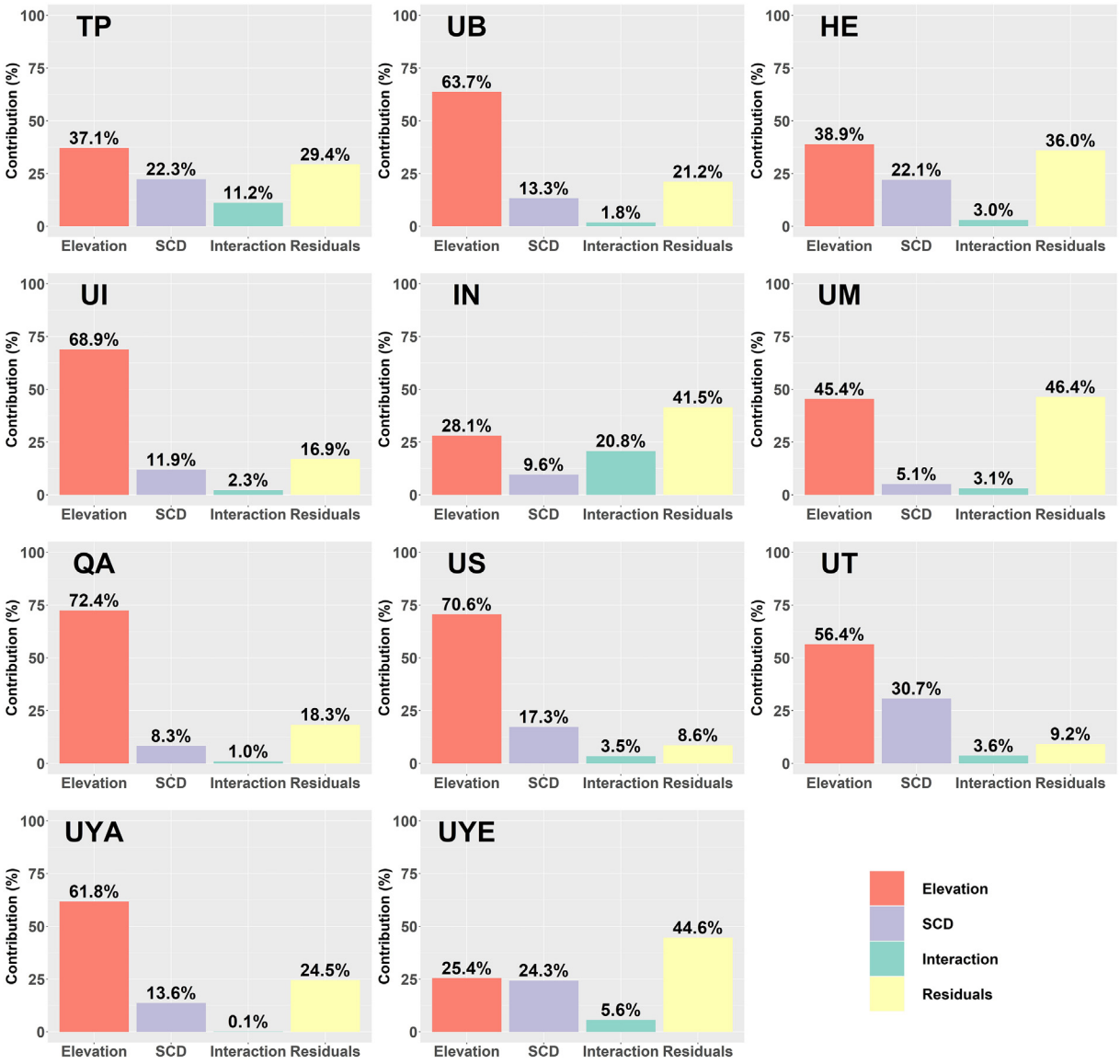

Fig. 7. Contributions of Elevation, SCD, their interaction term and the remaining residuals to the total variances of warming rates based on ANOVA for TP and 10 major basins. Note: The results for UA and UG with most pixels showing insignificant warming rates are not shown here due to insufficient samples.

variations of cloud cover and snow cover persistence. More clouds lead to decreased downward shortwave radiation and could thus inhibit warming (You et al., 2020), which is also consistent with Yang et al. (2018) who found less solar radiation received at higher elevations due to more clouds in the afternoon in the south of central Himalaya. Though previous studies paid more attention to the changing trends of cloud cover, vegetation and snow cover, our result implies that the climatological condition of these variables themselves could have important effects on the warming patterns.

The partial least squares path model (PLS-PM) was further used to distinguish their effects (Fig. 3b–d). Generally, snow cover persistence was the most important factor among them and it also presented the largest direct effect on warming for elevations of either below or above 5000 m. It is interesting that the total effect of elevation on warming was positive (0.19) for elevations below 5000 m whereas negative (−0.06) at elevations above 5000 m, which is highly consistent with the altitudinal patterns of warming rate. This indicates that the PLS-PM used here could at least partly explained such contrasting patterns. For elevations ≤5000 m, elevation did have a relatively high direct effect (0.34) on warming which could be attributed to the dominant mechanism of snow albedo feedback. Such a positive direct effect could balance over the negative indirect effect (−0.25) from snow cover persistence (Fig. 3c). The indirect effects from cloud cover (0.06) and NDVI (0.04) were relatively small. However, when elevation >5000 m, the direct effect of elevation was much lower (0.09) and the negative indirect effect from snow cover persistence was still large (0.20), leading to a negative total effect of elevation (Fig. 3d). It is also reasonable that the direct effect of NDVI was minimal as there are few vegetations at high elevations. Thus, the reversed altitudinal pattern of warming rates could be mainly due to the consistently high snow cover persistence at higher elevations.

3.4. The step-wise temperature increase and possible causes

It can be seen that the warming rate during 1980–2014 has been far from homogenous. The year 1997 seemed to be a distinct turning point with the warming trends for both the periods of 1980–1997 and 1998–2014 much lower than the entire period (Fig. 8) for the TP. This was further confirmed by the mostly insignificant trends for the periods 1980–1997 (Fig. 1b) and 1998–2014 (Fig. 1c), but highly significant trends when the entire period was considered (Fig. 1a). Interesting enough, the period around the year 1997 also coincides with other

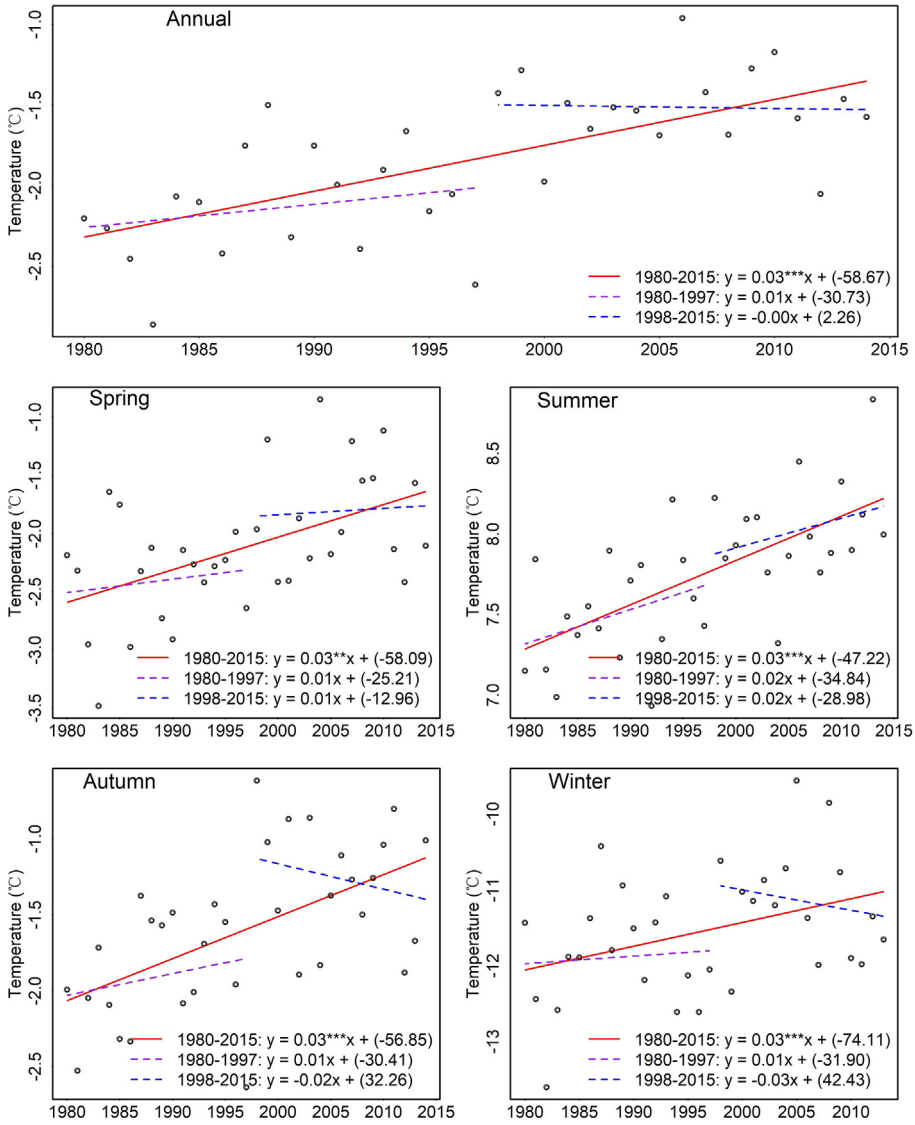

Fig. 8. Interannual variation of annual, spring, summer, autumn and winter air temperatures during 1980–2014 for TP. The trend lines based on linear regressions are also plotted. The red solid line represents the period of 1980–2014; the purple dashed line represents the period of 1980–1997 and the blue dashed line represents the period of 1998–2014. ***: $P < 0.001$; **: $P < 0.01$; *: $P < 0.05$.

evidence of abrupt environmental change such as the expansion of Tibetan lakes after 1997/1998 (Zhang et al., 2017), increased glacier melt(Maurer et al., 2019) and sediment flux (Zhang et al., 2020), and a decrease in permafrost area (Wang et al., 2019). The underlying reasons may be related to changes in large-scale atmospheric circulation (Zhang et al., 2017). Especially, the 1997–1998 El Niño, regarded as one of the strongest El Niño–Southern Oscillation events on record may have triggered an abrupt temperature change (Blunden and Arndt, 2016; Trenberth et al., 2002). This abrupt temperature change may have promoted an abrupt environmental change that acts as a positive feedback causing the temperature increase to persist and further exacerbate global warming rates. Although it may be too early to pinpoint the exact mechanism for this abrupt stepwise increase, a possible explanation chain is that more net energy is available for the sensible heat flux, because less energy is required to melt permafrost, glacier and snow. Furthermore, there was a well-established albedo feedback in the case of reduced snow cover. The average annual snow cover day (SCD) during 1980–2013 calculated using daily snow depth observations from 32 stations (Fig. 1a) showed a significantly decreasing trend (Fig. 9a), and the sequential Mann-Kendall test interestingly showed that 1997 and 2000 were two turning points (Fig. 9b) which showed a remarkable resemblance with the stepwise change in temperature. Although the annual stepwise warming was very obvious, its seasonality was rather complex. For the whole TP, similar stepwise warming after 1997 was observed in spring, autumn and winter, but less obvious in summer.

3.5. Uncertainties

Firstly, there is some uncertainty related to the new air temperature dataset. The validation accuracy (root-mean-squared-deviation) of the new dataset is reported to be 1.7 ± 0.3 °C, 1.8 ± 0.5 °C and 1.9 ± 0.7 °C for CMA stations (Number = 100), high-elevation stations (Number = 13), and glacier stations (Number = 4), respectively (Zhang et al., 2021). Such accuracy is considered relatively high compared with previous air temperature estimations with reported errors mostly around 2 °C (Rao et al., 2019; Zhang et al., 2016; Zhang et al., 2018a). In particular, the validation accuracy of the new dataset on glaciers is much higher than that of a previous air temperature estimation using Moderate Resolution Imaging Spectroradiometer (MODIS) land surface temperature (LST) (root-mean-squared-deviation >3 °C) which was conducted on the same four glaciers (Zhang et al., 2018b). The temporal

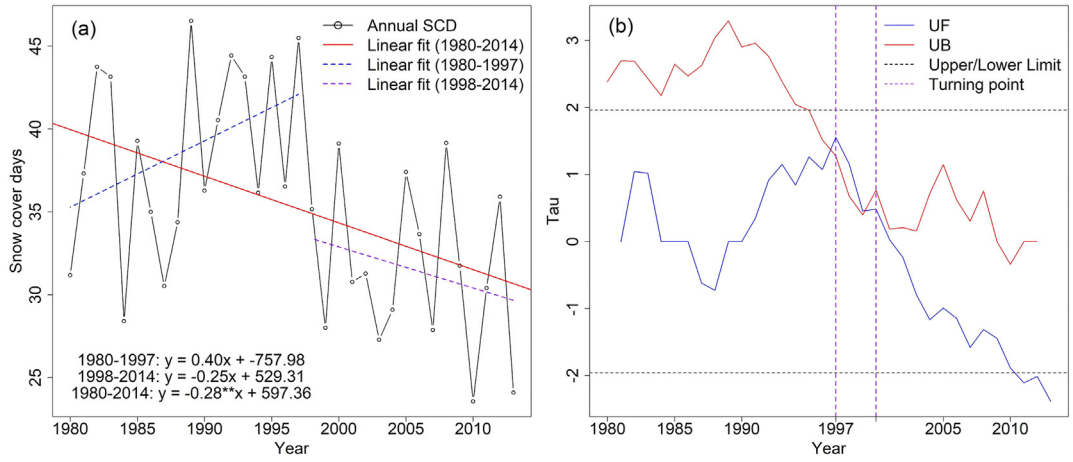

Fig. 9. The variation of snow cover days during 1980–2013 based on 32 stations (a) and the turning point of snow cover days from the sequential Mann-Kendall test (b). The crossing points of the positive series (UF) and the inverse series (UB) between the confidence limits are considered as turning points. It should be noted that the snow cover days shown here are calculated only based on the 32 stations. ***: $P < 0.001$; **: $P < 0.01$; *: $P < 0.05$.

trends calculated from the new dataset were also evaluated by comparison with those derived from eight reanalysis datasets and find that the former is very consistent with the best (i.e., the most accurate) two reanalysis datasets. However, it should be noted that there were only three stations higher than 5000 m used in the estimation and validation of the new temperature dataset and more observation from high-elevation stations should be collected in future to increase the representativeness in elevation for air temperature estimation. The detailed results about comparison and validation against eight reanalysis datasets can be found in Zhang et al. (2021). Compared with the reanalysis datasets with generally coarser resolution, the new dataset with much higher spatial resolution and validation accuracy is expected to produce more reliable warming rates of TP. Furthermore, we also acknowledge that the long-term microwave-based snow depth dataset with relatively coarse resolution (see Section 2.1) could bring some uncertainty. Although it seemed to overestimate SCD of the TP, its multiyear average SCD during 2005–2013 shows a similar spatial pattern to that of MODIS-based snow cover data (not shown here), and its annual snow cover days during 1980–2013 also had a relatively high and significant ($P < 0.001$) Pearson correlation coefficient of ~0.6 with those based on the 32 stations. In addition, the decreasing rates of SCD from station-based (−2.8 day/10a) (Fig. 9a) and satellite-based (−4.0 day/10a) data were similar. In addition, the cloud cover and NDVI data used in this study may have some uncertainty due to the errors from detection and removal of clouds during their production process. However, such effects may not be big because elevation and snow cover persistence were demonstrated to be two major factors controlling the warming patterns (Fig. 4).

There may also be some uncertainty in the approach for analyzing effects of snow cover persistence on TP warming. The short period (2005–2013) of SCD data was a limitation that the derived multiyear average SCD may have some uncertainty in the representativeness for the whole study period (1980–2014). Reliable Long-term snow cover data with high resolutions are thus needed to be developed in future for better estimating multiyear average SCDs and SCD trends of the long period. It is also difficult for this approach to exactly distinguish the effect of glaciers from that of snow. On the one hand, glacier surfaces are often covered by snow while the remote sensing snow cover data used cannot distinguish glacier from snow; on the other hand, glaciers have obviously lower albedo than snow further adding the complexity for distinguishing their effects. Thus, more efforts may be needed in future to analyze the combined effects of snow cover and glacier by comprehensively using remote sensing and modeling approaches. In addition to snow cover, clouds and NDVI, winds and air water vapor (Rangwala et al., 2010; Rangwala et al., 2009) may also have significant effects on TP warming. Future studies are thus needed to develop high-resolution long-term datasets of wind speed and air water vapor for achieving a more comprehensive analysis. Another uncertainty is related with the ANOVA. As mentioned in Section 2.2, the two-way ANOVA was conducted in four sub-regions separately and the results could be very different among the sub-regions. The detailed ANOVA results for all the four sub-regions in the 11 major basins were thus examined. It is reasonable that for each basin, the weighted average contribution of each component was more similar to that of the sub-region with the largest coverage in Fig. 6, although the results are not shown here.

4. Conclusions

Our high-resolution temperature dataset allowed us to confirm with high confidence that most major TP basins warm rapidly, in particular in winter. Notable stepwise warming in annual temperature change is detected in 1997 although the seasonality is rather complex. Such abrupt warming can explain some observed sudden environmental changes starting in the late 1990s. Overall, EDW is only valid up to about 5000 m above which the persistent snow cover prohibits an increase of warming rate with increasing height, making the altitudinal patterns of elevations below and above 5000 m reversed. For the first time, the new data covers elevations above 5000 m with the best accuracy reached so far, which made it possible for us to conclude that the well-established snow-albedo feedback is less important at high elevations than in low-middle elevation areas, because of the persistent existence of snow covers at high elevations. The hardly changed snow covered and glacierized areas over high elevations effectively constrain the warming rates. There is an important positive feedback loop and warming rates are amplified when snow cover and glacier areas are reduced. Thus, with the depletion of snow cover and glaciers, more prominent warming may occur on the TP in the future which could further enhance other environmental changes. The feedback of both snow and glacier changes on warming should also be considered in future regional climate change predictions.

Data availability

The 1-km daily air temperature dataset of the Tibetan Plateau during 1980–2014 can be obtained from http://data.tpdc.ac.cn/en/data/62234872-c39c-4614-a7ac-348c9437e7d5 with doi number: 10.11888/Meteoro.tpdc.270377.

CRediT authorship contribution statement

All authors made significant contributions to this study. W.W.I., H.Z., F.Z. and D.C. designed this study; H.Z. performed all analyses; H.Z., W.W.I. and F.Z. wrote the manuscript; R.J.d.K., D.C. and W.Y. discussed the results, commented on the manuscript and contributed to writing.

Declaration of competing interest

Authors declare that they have no conflict of interest.

Acknowledgements

This study was supported by the Second Tibetan Plateau Scientific Expedition and Research Program (2019QZKK0203), the "Strategic Priority Research Program" of the Chinese Academy of Sciences (XDA20060202), the National Natural Science Foundation of China (Grant No. 41701079), the Talent Cultivation and Development Support Program by China Agricultural University (Li Sien) and the China Scholarship Council.

References

Blunden, J., Arndt, D.S., 2016. State of the climate in 2015. Bull. Am. Meteorol. Soc. 97, Si-S275.
Brun, F., Berthier, E., Wagnon, P., Kääb, A., Treichler, D., 2017. A spatially resolved estimate of High Mountain Asia glacier mass balances from 2000 to 2016. Nat. Geosci. 10, 668.
Che, T., Li, X., Jin, R., Armstrong, R., Zhang, T.J., 2008. Snow depth derived from passive microwave remote-sensing data in China. (2008). In: Schneebeli, M. (Ed.), Annals of Glaciology. Vol 49. Int Glaciological Soc, Cambridge, pp. 145–154.
Cheng, G., Wu, T., 2007. Responses of permafrost to climate change and their environmental significance, Qinghai-Tibet plateau. J. Geophys. Res. Earth Surf. 112.
Dai, L., Che, T., Wang, J., Zhang, P., 2012. Snow depth and snow water equivalent estimation from AMSR-E data based on a priori snow characteristics in Xinjiang, China. Remote Sens. Environ. 127, 14–29.
Didan, K., Munoz, A.B., Solano, R., Huete, A., 2015. MODIS Vegetation Index User's Guide (MOD13 Series). University of Arizona: Vegetation Index and Phenology Lab.
Ding, L., Zhou, J., Zhang, X., Liu, S., Cao, R., 2018. Downscaling of surface air temperature over the tibetan plateau based on DEM. Int. J. Appl. Earth Obs. Geoinf. 73, 136–147.
Duan, A., Wu, G., 2006. Change of cloud amount and the climate warming on the Tibetan plateau. Geophys. Res. Lett. 33.
Duan, J., Li, L., Fang, Y., 2015. Seasonal spatial heterogeneity of warming rates on the Tibetan plateau over the past 30 years. Sci. Rep. 5, 1–8.
Fowler, H., Archer, D., 2006. Conflicting signals of climatic change in the upper Indus Basin. J. Clim. 19, 4276–4293.
Gao, Y., Chen, F., Lettenmaier, D.P., Xu, J., Xiao, L., Li, X., 2018. Does elevation-dependent warming hold true above 5000 m elevation? Lessons from the Tibetan plateau. NPJ Clim. Atmos. Sci. 1, 19.
Gao, K., Duan, A., Chen, D., Wu, G., 2019. Surface energy budget diagnosis reveals possible mechanism for the different warming rate among Earth's three poles in recent decades. Sci. Bull. 64, 1140–1143.
Gardelle, J., Berthier, E., Arnaud, Y., 2012. Slight mass gain of Karakoram glaciers in the early twenty-first century. Nat. Geosci. 5, 322.
Guo, D., Wang, H., 2012. The significant climate warming in the northern Tibetan plateau and its possible causes. Int. J. Climatol. 32, 1775–1781.
Guo, D., Yu, E., Wang, H., 2016. Will the Tibetan plateau warming depend on elevation in the future? J. Geophys. Res. Atmos. 121, 3969–3978.
Guo, D., Sun, J., Yang, K., Pepin, N., Xu, Y., 2019a. Revisiting recent elevation-dependent warming on the Tibetan plateau using satellite-based data sets. J. Geophys. Res. Atmos. 124, 8511–8521.
Guo, D., Sun, J., Yang, K., Pepin, N., Xu, Y., Xu, Z., et al., 2019b. Satellite data reveal southwestern tibetan plateau cooling since 2001 due to snow-albedo feedback. Int. J. Climatol. 40, 1644–1655.
Guo, D., Pepin, N., Yang, K., Sun, J., Li, D., 2021. Local changes in snow depth dominate the evolving pattern of elevation-dependent warming on the Tibetan plateau. Sci. Bull. 66 (11), 1146–1150.
Hector, A., Von Felten, S., Schmid, B., 2010. Analysis of variance with unbalanced data: an update for ecology & evolution. J. Anim. Ecol. 79, 308–316.
Hewitt, K., 2005. The Karakoram anomaly? Glacier expansion and the 'elevation effect,' Karakoram Himalaya. Mt. Res. Dev. 25, 332–341.
Hua, S., Liu, Y., Jia, R., Chang, S., Wu, C., Zhu, Q., et al., 2018. Role of clouds in accelerating cold-season warming during 2000–2015 over the Tibetan plateau. Int. J. Climatol. 38, 4950–4966.
Immerzeel, W.W., van Beek, L.P.H., Bierkens, M.F.P., 2010. Climate change will affect the Asian water towers. Science 328, 1382–1385.
Kang, S., Zhang, Q., Qian, Y., Ji, Z., Li, C., Cong, Z., et al., 2019. Linking atmospheric pollution to cryospheric change in the third pole region: current progress and future prospects. Natl. Sci. Rev. 6, 796–809.
Kapnick, S.B., Delworth, T.L., Ashfaq, M., Malyshev, S., Milly, P.C., 2014. Snowfall less sensitive to warming in Karakoram than in Himalayas due to a unique seasonal cycle. Nat. Geosci. 7, 834.
Li, B., Chen, Y., Shi, X., 2020. Does elevation dependent warming exist in high mountain Asia? Environ. Res. Lett. 15.
Lin, H., Li, G., Cuo, L., Hooper, A., Ye, Q., 2017. A decreasing glacier mass balance gradient from the edge of the upper Tarim Basin to the Karakoram during 2000–2014. Sci. Rep. 7, 6712.
Liu, X., Chen, B., 2000. Climatic warming in the Tibetan plateau during recent decades. Int. J. Climatol. 20, 1729–1742.
Liu, Y., Zhang, Y., Zhu, J., Huang, K., Zu, J., Chen, N., et al., 2019. Warming slowdown over the tibetan plateau in recent decades. Theor. Appl. Climatol. 135, 1375–1385.
Liyun, D., Tao, C., 2015. In: National Tibetan Plateau Data, C. (Ed.), Long-term Series of Daily Snow Depth Dataset in China (1979-2020). National Tibetan Plateau Data Center.
Maurer, J., Schaefer, J., Rupper, S., Corley, A., 2019. Acceleration of ice loss across the Himalayas over the past 40 years. Sci. Adv. 5, eaav7266.
Nie, Y., Han, X., Chen, J., Wang, M., Shen, W., 2019. The simulated N deposition accelerates net N mineralization and nitrification in a tropical forest soil. Biogeosciences 16, 4277–4291.
Niu, X., Tang, J., Chen, D., Wang, S., Ou, T., 2021. Elevation-dependent warming over the Tibetan plateau from an ensemble of CORDEX-EA regional climate simulations. J. Geophys. Res. Atmos. 126, e2020JD033997.
Palazzi, E., Filippi, L., von Hardenberg, J., 2017. Insights into elevation-dependent warming in the Tibetan plateau-Himalayas from CMIP5 model simulations. Clim. Dyn. 48, 3991–4008.
Palazzi, E., Mortarini, L., Terzago, S., von Hardenberg, J., 2019. Elevation-dependent warming in global climate model simulations at high spatial resolution. Clim. Dyn. 52, 2685–2702.
Peng, S., Ding, Y., Liu, W., Li, Z., 2019. 1 km monthly temperature and precipitation dataset for China from 1901 to 2017. Earth Syst. Sci. Data 11, 1931–1946.
Pepin, N., Bradley, R., Diaz, H., Baraër, M., Caceres, E., Forsythe, N., et al., 2015. Elevation-dependent warming in mountain regions of the world. Nat. Clim. Chang. 5, 424–430.
Pepin, N., Deng, H., Zhang, H., Zhang, F., Kang, S., Yao, T., 2019. An examination of temperature trends at high elevations across the Tibetan plateau: the use of MODIS LST to understand patterns of elevation-dependent warming. J. Geophys. Res. Atmos. 124, 5738–5756.
Pfeffer, W.T., Arendt, A.A., Bliss, A., Bolch, T., Cogley, J.G., Gardner, A.S., et al., 2014. The Randolph glacier inventory: a globally complete inventory of glaciers. J. Glaciol. 60, 537–552.
Qin, J., Yang, K., Liang, S., Guo, X., 2009. The altitudinal dependence of recent rapid warming over the Tibetan plateau. Clim. Chang. 97, 321.
Rangwala, I., Miller, J.R., Xu, M., 2009. Warming in the tibetan plateau: possible influences of the changes in surface water vapor. Geophys. Res. Lett. 36.
Rangwala, I., Miller, J.R., Russell, G.L., Xu, M., 2010. Using a global climate model to evaluate the influences of water vapor, snow cover and atmospheric aerosol on warming in the Tibetan plateau during the twenty-first century. Clim. Dyn. 34, 859–872.
Rao, Y., Liang, S., Wang, D., Yu, Y., Song, Z., Zhou, Y., et al., 2019. Estimating daily average surface air temperature using satellite land surface temperature and top-of-atmosphere radiation products over the Tibetan plateau. Remote Sens. Environ. 234, 111462.
Sanchez, G., 2013. PLS Path Modeling With R. Trowchez Editions, Berkeley, p. 383 (2013).
Shen, M., Piao, S., Jeong, S.-J., Zhou, L., Zeng, Z., Ciais, P., et al., 2015. Evaporative cooling over the Tibetan plateau induced by vegetation growth. Proc. Natl. Acad. Sci. 112, 9299–9304.
Takala, M., Luojus, K., Pulliainen, J., Derksen, C., Lemmetyinen, J., Kärnä, J.-P., et al., 2011. Estimating northern hemisphere snow water equivalent for climate research through assimilation of space-borne radiometer data and ground-based measurements. Remote Sens. Environ. 115, 3517–3529.
Team G, 2016. GISS surface temperature analysis (GISTEMP). NASA Goddard Institute for Space Studies. Dataset https://data. giss. nasa. gov/gistemp.
Trenberth, K.E., Caron, J.M., Stepaniak, D.P., Worley, S., 2002. Evolution of El Niño-southern oscillation and global atmospheric surface temperatures. J. Geophys. Res. Atmos. 107 (AAC 5-1-AAC 5–17).
Wang, T., Wu, T., Wang, P., Li, R., Xie, C., Zou, D., 2019. Spatial distribution and changes of permafrost on the Qinghai-Tibet plateau revealed by statistical models during the period of 1980 to 2010. Sci. Total Environ. 650, 661–670.
Wilson, A.M., Jetz, W., 2016. Remotely sensed high-resolution global cloud dynamics for predicting ecosystem and biodiversity distributions. PLoS Biol. 14, e1002415.
Wu, G., Liu, Y., Zhang, Q., Duan, A., Wang, T., Wan, R., et al., 2007. The influence of mechanical and thermal forcing by the Tibetan plateau on Asian climate. J. Hydrometeorol. 8, 770–789.
Yang, W., Yao, T., Guo, X., Zhu, M., Li, S., Kattel, D.B., 2013. Mass balance of a maritime glacier on the southeast Tibetan plateau and its climatic sensitivity. J. Geophys. Res. Atmos. 118, 9579–9594.
Yang, K., Guyennon, N., Ouyang, L., Tian, L., Tartari, G., Salerno, F., 2018. Impact of summer monsoon on the elevation-dependence of meteorological variables in the south of central Himalaya. Int. J. Climatol. 38, 1748–1759.
Yao, T., Thompson, L., Yang, W., Yu, W., Gao, Y., Guo, X., et al., 2012. Different glacier status with atmospheric circulations in Tibetan plateau and surroundings. Nat. Clim. Chang. 2, 663–667.
You, Q., Kang, S., Pepin, N., Yan, Y., 2008. Relationship between trends in temperature extremes and elevation in the eastern and central Tibetan plateau, 1961–2005. Geophys. Res. Lett. 35.

You, Q., Chen, D., Wu, F., Pepin, N., Cai, Z., Ahrens, B., et al., 2020. Elevation dependent warming over the Tibetan plateau: patterns, mechanisms and perspectives. Earth Sci. Rev. 210, 103349.

You, Q., Cai, Z., Pepin, N., Chen, D., Ahrens, B., Jiang, Z., et al., 2021. Warming amplification over the Arctic pole and third pole: trends, mechanisms and consequences. Earth Sci. Rev. 217, 103625.

Yu, J., Zhang, G., Yao, T., Xie, H., Zhang, H., Ke, C., et al., 2016. Developing daily cloud-free snow composite products from MODIS Terra-aqua and IMS for the Tibetan plateau. IEEE Trans. Geosci. Remote Sens. 54, 2171–2180.

Zhang, H., Zhang, F., Ye, M., Che, T., Zhang, G., 2016. Estimating daily air temperatures over the Tibetan plateau by dynamically integrating MODIS LST data. J. Geophys. Res. Atmos. 121, 11425–11441.

Zhang, G., Yao, T., Piao, S., Bolch, T., Xie, H., Chen, D., et al., 2017. Extensive and drastically different alpine lake changes on Asia's high plateaus during the past four decades. Geophys. Res. Lett. 44, 252–260.

Zhang, H., Zhang, F., Zhang, G., Che, T., Yan, W., 2018a. How accurately can the air temperature lapse rate over the Tibetan plateau be estimated from MODIS LSTs? J. Geophys. Res. Atmos. 123, 3943–3960.

Zhang, H., Zhang, F., Zhang, G., Ma, Y., Yang, K.U.N., Ye, M., 2018b. Daily air temperature estimation on glacier surfaces in the Tibetan plateau using MODIS LST data. J. Glaciol. 1–16.

Zhang, G., Yao, T., Chen, W., Zheng, G., Shum, C.K., Yang, K., et al., 2019. Regional differences of lake evolution across China during 1960s–2015 and its natural and anthropogenic causes. Remote Sens. Environ. 221, 386–404.

Zhang, F., Shi, X., Zeng, C., Wang, L., Xiao, X., Wang, G., et al., 2020. Recent stepwise sediment flux increase with climate change in the Tuotuo River in the central Tibetan plateau. Sci. Bull. 65, 410–418.

Zhang, H., Immerzeel, W.W., Zhang, F., de Kok, R., Gorrie, J.S., Ye, M., 2021. Creating 1-km long-term (1980–2014) daily average air temperatures over the tibetan plateau by integrating eight types of reanalysis and land data assimilation products downscaled with MODIS-estimated temperature lapse rates based on machine learning. Int. J. Appl. Earth Obs. Geoinf. 97, 102295.